Article

SAARIMAA et al.Assessment of pitting corrosion in bare and passivated (wet $scCO_2$-induced patination and chemical passivation) hot-dip galvanized steel samples with SVET, FTIR, and SEM (EDS)

Ville Saarimaa[a,*], Nuria Fuertes[b], Dan Persson[c], Tommy Zavalis[c], Aaretti Kaleva[d], Juha-Pekka Nikkanen[d], Erkki Levänen[d], Golrokh Heydari[e]

Top Analytica, Turku, Finland

Swerim AB, Kista, Sweden

~~RISE,~~ Division Materials and Production, RISE, Kista, Sweden

Materials Science and Environmental Engineering, Tampere University, Tampere, Finland

SSAB Europe, Kista, Sweden

**Correspondence** Ville Saarimaa, Top Analytica, Ruukinkatu 4, FI-20540 Turku, Finland. Email: ville.saarimaa@topanalytica.com

03/09/2020; 04/24/2020; 05/06/2020

# Abstract

In this study, the local electrochemical activity of untreated and passivated (natural or chemical passivation) zinc specimens was observed during immersion in a 0.1-M NaCl solution. The localized anodic activity during the exposure, measured with the scanning vibrating electrode technique, was linked to zinc dissolution by the pitting corrosion mechanism. It was correlated to specific corrosion products characterized by Fourier transmission infrared (FTIR) microscopy. FTIR molecule maps were produced from individual pitting corrosion sites (100–200 μm in width). With argon ion beam milling and latest energy-dispersive X-ray spectroscopy (EDS) technology, element maps with a high spatial resolution (≪100 nm) were recorded from abrasion- and beam-sensitive corrosion products, showing a residual layer structure. This study demonstrates the capability of FTIR mapping, cross-section polishing, and state-of-the-art scanning electron microscopy imaging, and EDS element mapping to produce high-resolution elemental, molecular, and visual information about pitting corrosion mechanisms on a hot-dip galvanized steel sample.

# Graphical abstract

Salt-induced pitting corrosion of hot-dip galvanized steel can be suppressed by suitable passivating layers. Such layers can function by withstanding ion-exchange reactions or reducing ionic diffusion through the barrier layer. A combination of local electrochemical measurements with molecular spectroscopy and high-resolution cross-section element mapping can clarify the root cause for

pitting corrosion and facilitate tailoring of appropriate protective layers for specific environments.

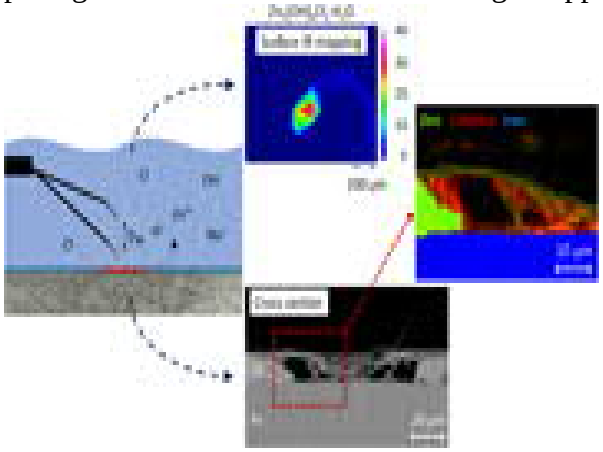

fx1


# KEYWORDS

anodic dissolution, FTIR microscopy, passivation, pitting corrosion, scanning electron microscopy, zinc


# INTRODUCTION

The hot-dip galvanized (HDG) steel is a widely used raw material in the construction industry. There are different standard procedures for evaluation of corrosion resistance of zinc coatings, such as accelerated atmospheric corrosion testing in climate chambers or electrochemical testing such as potentiometric measurements and electrochemical impedance spectroscopy. However, these methods yield average information about the corrosion resistance of the coatings, without differentiating their local activity correlated to barrier properties and various corrosion products. A better understanding of the local barrier properties of the coatings would contribute to the development of more resistant protective coatings. Modern electrochemical and characterization techniques can provide information about local (micrometer scale) electrochemical corrosion processes (oxidoreduction reactions) taking place on the specimen surface. The scanning vibrating electrode technique (SVET) is a microelectrochemical technique that allows the mapping of current density variations over a corroding specimen surface immersed in an electrolyte. It has been used in numerous investigations to study corrosion of metals, such as pitting corrosion, oxide dissolution, and corrosion of coatings.[1–5] Pitting corrosion is one of the main corrosion mechanisms that can take place in zinc coatings, resulting in the local dissolution of zinc and the formation of singular cavities.[6] Typically, the rest of the metal surface suffers very little dissolution. On passive metal surfaces, aggressive species, such as chloride ions, can locally break down the passive surface. The composition and distribution of corrosion products on a corroding metal surface are strongly related to the chemical conditions that prevail during the corrosion process. For instance, the local pH and distribution of ions on a corroding metal surface are strongly related to the local electrochemical processes, which lead to local variations in the corrosion product composition. Thus, the composition and distribution of corrosion products on a surface reveal important information about the corrosion processes and mechanisms. Fourier transmission infrared (FTIR) spectroscopy is a powerful technique for the chemical analysis, and it provides information about the molecular species and phases in a sample as well as information about chemical bonding and interaction. FTIR

microscopical mapping and imaging have been used in several studies to obtain information about the composition and distribution of corrosion products on zinc-coated steel.[7,8] The latest advancements in energy-dispersive X-ray spectroscopy (EDS) have remarkably improved the sensitivity of elemental mapping, even for beam-sensitive materials that require the utilization of low accelerating voltages. For zinc coatings, nm-scale spatial resolution has been achieved.[9] Argon ion beam milling is capable of producing high-quality cross-sections of very thin layers (<100 nm) and abrasion-sensitive deposits on zinc coatings.[10–12]

In this study, HDG steel samples (unprotected and protected by passivating layers) were immersed in a 0.1-M NaCl solution to induce localized corrosion attack (pitting corrosion). The electrochemical activity was recorded by SVET. Detailed pitting corrosion mechanisms are well covered in the literature.[6] The purpose of this investigation was to demonstrate how modern FTIR mapping, high-quality cross-section preparation (ion beam milling), scanning electron microscopy (SEM) imaging, and EDS element analysis can contribute to a better understanding of the pitting corrosion processes, either on bare zinc coatings or on passivated specimens.

# MATERIALS AND METHODS

## Materials

In this study, HDG steel (0.2 wt% Al in the zinc bath) with a total zinc coating mass of 275 g/m$^2$ from SSAB Europe was used. The material was nonoiled. An accelerated zinc patina growth was achieved in wet supercritical carbon dioxide.[13] The passivated samples were obtained applying a commercial $Cr^{3+}$-based passivation solution on HDG according to the manufacturer's instructions (Gardolene D6812, Chemetall). The sample specification is provided in OTable 1, and SEM cross-section images and EDS element maps of unexposed samples are shown in OFigure 1.

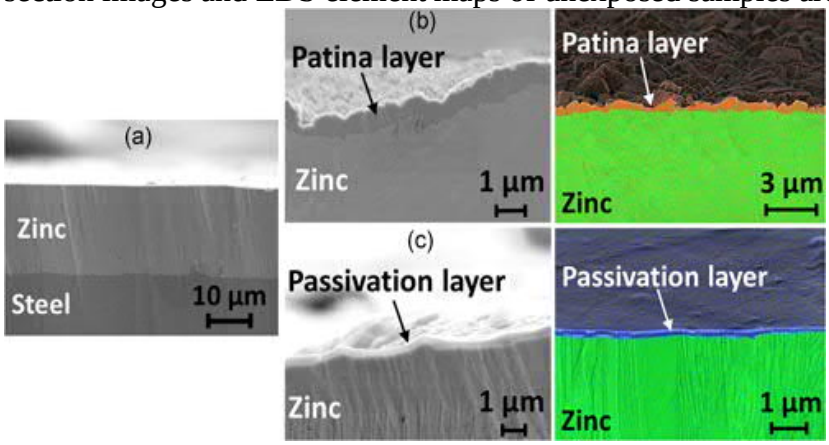


Scanning electron microscopy cross-section images of the samples before exposure. (a) Untreated hot-dip galvanized (HDG). (b) Patinated HDG. (c) Passivated HDG. In energy-dispersive X-ray spectroscopy element maps, Zn is green, O is red, and Cr is blue

List of samples

| | Name | Surface treatment | Surface composition | Approx. layer thickness |
|---|---|---|---|---|
| A | Untreated HDG | – | – | – |
| B | Patinated HDG | $ScCO_2$ treatment (5 ml $H_2O$, 80 bar, 60°C, 1 hr)[12] | $ZnCO_3$ | 1.0 µm |
| C | Passivated HDG | Gardolene D6812 (Chemetall) | $Cr_2O_3$ | 0.3 µm |

Abbreviation: HDG, hot-dip galvanized.

# NaCl immersion tests

Samples with dimensions 2.5 × 3.0 cm were coated with Lacomit varnish (Agar Scientific), leaving a 1.0 × 1.5 cm area uncoated. The samples were fully immersed in 30 ml of a 0.1-M NaCl solution in separate beakers. Parallel samples were exposed. The number of black spots (pits) was observed after 3, 6, 24, 48, and 72 hr. After each immersion interval, the samples were rinsed with DI water, dried with pressurized air, and studied by optical light microscopy. The NaCl solution was changed after 24-hr immersion.

# SVET measurements

The SVET measurements were carried out with equipment manufactured by Applicable Electronics Inc., using a microelectrode (probe) of an isolated platinum wire. The probe was electroplated with a platinum black ball of a diameter 2–50 µm. During the measurement, the tip of the electrode was immersed in the electrolyte and vibrated vertically in a sine wave of 150 ± 10 µm over the specimen surface, which was also immersed in the electrolyte. The SVET set-up acted like a capacitor where the two conductors, the working electrode (specimen) and the electrode, were placed in parallel with a certain distance between them, which was dependent on the vertical vibration of the electrode. The electrode measured the potential drop between the top and the bottom of the vibration waves, $\nabla\phi$, associated with corrosion ionic current originated from the surface of the specimen. The measured $\nabla\phi$ signal was subsequently filtered and amplified through x/y phase detectors, converting the AC signal to a DC potential. As given in Equation (1), the current density $i$ was calculated by Ohm's law using the potential drop ($\nabla\phi$) and the conductivity of the electrolyte ($-k$):$i = -k \cdot \nabla\phi.$

The current density was plotted for each mesh point of the SVET scan, resulting in a current density map. Anodic currents, correlated to oxidation processes, were positive values and cathodic currents, correlated to reduction processes, corresponded to the negative values. The quality control of the microelectrode was carried out before each measurement session by verifying a capacitance value of at least 2 nF. All experiments were carried out at the open-circuit potential and in a 0.1-M NaCl solution.

The samples (with 3 × 4-mm exposed surface and the surrounding surface insulated with Lacomit varnish, Agar Scientific) were exposed in the 0.1-M NaCl solution for two 6-hr periods over 2 days. At the end of both periods, the solution was removed and the samples were quickly rinsed with distilled water. The samples were dried overnight (for 18 hr) between the two exposure periods. The SVET scans were performed at the beginning and the end of each period. An SVET scan took about 25 min. Parallel samples were exposed to confirm the results.

## FTIR microscopy

FTIR focal plane array mapping was performed using the Vertex 70 spectrometer with a Hyperion 3000 microscope and a wideband single-point MCT (Mercury–Cadmium–Telluride) detector (cut-off at 400 $cm^{-1}$). The measurements were performed using a 15X Cassegrain objective, adding 256 scans for each measurement. The resolution was 8 $cm^{-1}$. The measurements were performed using a 100 × 100-μm aperture.

## SEM characterization

The SEM characterization was performed using a Zeiss Gemini 450 instrument, and the element composition mapping was performed using a Bruker QUANTAX FlatQUAD EDS system. Cross-sections for SEM characterization were prepared using an Ilion+ Advantage Precision Cross-Section System (Model 693; Gatan Inc.).

# RESULTS AND DISCUSSION

## Initiation of pitting corrosion in NaCl immersion

The reactivity of the samples (pitting corrosion tendency) was evaluated by a visual observation of the number of black spots per $cm^2$ as a function of time in an NaCl immersion. OFigure 2 shows the number of initiations that will develop into stable pits. The untreated HDG was very prone to pitting corrosion. The initial protective properties of HDG are due to the uniformly covering, inert $Al_2O_3$ layer on the surface.[9] However, the corrosion protection achieved by natural simple oxides is short lived. The corrosion processes were visibly continuous after 3-hr immersion, and with time, the formation rate of pits (black spots detectable with light microscopy) decreased remarkably. This is due to passivation of the active surface sites by the formation of corrosion products. The reactivity of exposed zinc decreases with time due to the spontaneous passivation of zinc by molecular oxide layers.[14] The corrosive sites will then convert into stable zinc patina, zinc hydroxy carbonates, and zinc hydroxy chloride, accounting for the main corrosion products.[7,15,16] The naturally forming zinc patina passivates metallic zinc and, in the long run, reduces the reactivity of HDG steel.[17–19] On the basis of the visual observation, both the patinated sample and the passivated sample fully protected the zinc surface at very short immersion times. Also, the number of black spots per $cm^2$

observed at the end of the test was lower than for the untreated HDG sample (Figure 2).

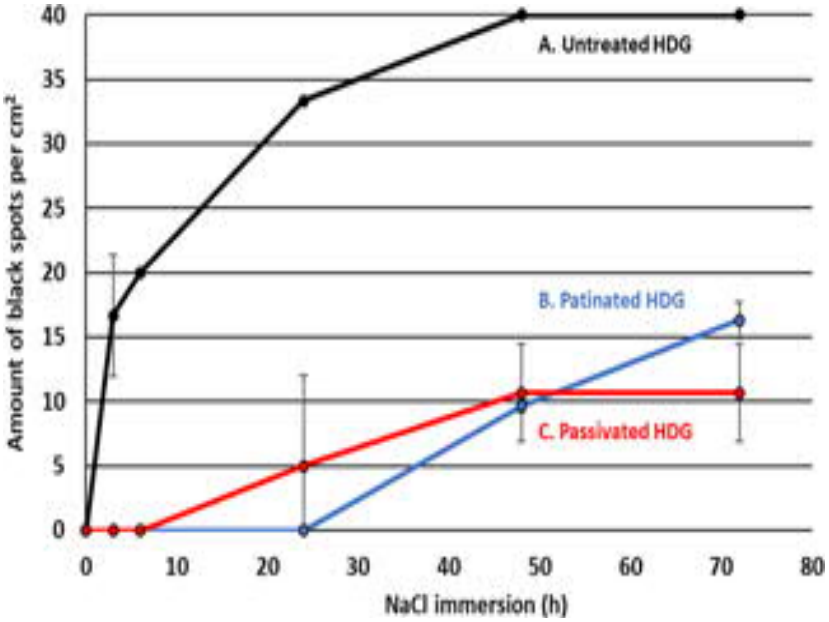


The evolution of pitting corrosion in unprotected and protected hot-dip galvanized samples as a function of time

The SVET tests were performed in similar conditions (0.1-M NaCl bath), but with the smaller exposed area to decrease the current density mapping time. In OFigure 3, SVET current maps of HDG samples are shown at different times of immersion in the SVET set-up. In the SVET current density maps, it can be observed that both cathodic (negative current) and anodic (positive current) regions were present. Large anodic and cathodic regions were developed and intensified during the immersion of the unprotected HDG sample and the patinated sample, whereas the passivated sample showed only very minor anodic currents. On day 2, an extensive anodic activity was observed at the same locations as the previous day. This activity even caused some interference in the measurements in the nearby regions. Some shifting of the anodic and cathodic locations occurred during the exposure. A likely explanation is the formation of several new locations of corrosion attack. The changes in locations of anodic regions between days 1 and 2 could be due to repassivation during the overnight drying or a possible formation of new corrosion attack sites. The anodic regions can contain several microscopic corrosion sites, which were not individually seen in the SVET current maps due to the resolution constraints of the method. For the patinated HDG sample, the electrochemical activity recorded with SVET (Figure 3) is much higher than that indicated by the number of pit initiations (Figure 2). This could be explained by electrochemical processes beneath the (initially) protective surface layer that was not observed by light microscopy from the top view until the last stages of observation. This is discussed more in detail later within the cross-sectional characterization of the samples (Figure 7). Although the anodic and cathodic currents were already observed at the beginning of the exposure for the patinated sample, it is noteworthy that the magnitude of the anodic current density was decreased during the second-day exposure, contrary to the untreated HDG sample where the anodic current density is fortified during the whole course of the exposure. The passivated sample showed only minor current densities,

conforming with the number of pit initiations (Figure 2).

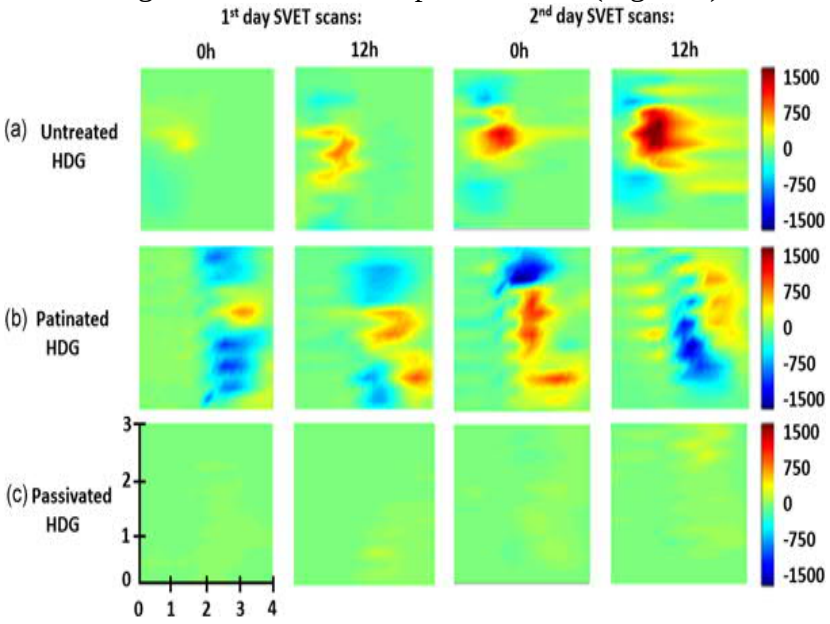


The electrochemical activity on hot-dip galvanized samples at different immersion times in the scanning vibrating electrode technique set-up. Units: a color legend in μA/cm$^2$ and spatial coordinates in mm. The positive values (red) are anodic currents and the negative values (blue) are cathodic currents

# FTIR microscopy

OFigure 4 shows FT-IRR spectra measured at black spots on the surface associated with anodic areas in the SVET measurement of sample A (untreated HDG). The spectrum P2 shows the formation of $Zn_5(OH)_8Cl_2 \cdot H_2O$ (simonkolleite, SC) at the anodic spots of the sample. The formation of $Zn_5(OH)_6(CO_3)$ (hydrozincite, HC) was also observed. In addition, the formation of $NaCO_3$ (sodium carbonate, NC) is indicated in the spectrum P1. The formation of this compound is probably associated with cathodic areas on the surface, where high pH values can develop during corrosion. This is consistent with the presence of cathodic areas close to the anodic spot in the SVET measurements in Figure 3. The interpretations of the spectra were based on the reference

spectra of zinc compounds presented in previous publications.[16,20]

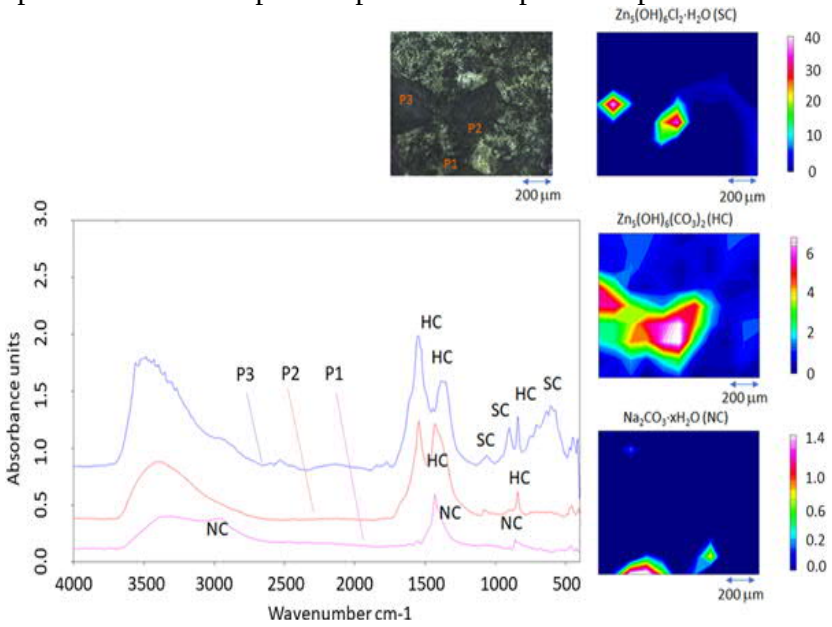


FTIR-IRR spectra and FTIR–FPA images of sample A (untreated hot-dip galvanized) after 2 days of exposure. The three spectra correspond to different measurement points in the light microscopy image (P1–P3), and the intensity maps of the main corrosion products in the measurement area are shown. FPA, focal plane array; FTIR, Fourier transmission infrared; HC, hydrozincite; NC, sodium carbonate; SC, simonkolleite

FTIR mapping on the patinated sample shows that $Zn_5(OH)_8Cl_2 \cdot H_2O$ and $Zn_5(OH)_6(CO_3)_2$ are found at a black spot area (OFigure 5). $Zn_5(OH)_8Cl_2 \cdot H_2O$ is located more in the central part of the area covered with corrosion products, whereas $Zn_5(OH)_6(CO_3)_2$ is less localized and found over the whole corrosion product-covered area. The formation of $Zn_5(OH)_8Cl_2 \cdot H_2O$ is consistent with the presence of an anodic area in the central part of the area with the corrosion products, as $Zn_5(OH)_8Cl_2 \cdot H_2O$ is more stable at low and intermediate pH conditions and higher chloride concentrations, whereas the formation of $Zn_5(OH)_6(CO_3)_2$ should take place when the pH increases toward the cathodic zones on the corroding surface.[15,21] There also seems to be a decrease in the intensity of the band due to the original patina component, $ZnCO_3$, in the area with the corrosion products. However, as seen from SEM images (Figure 7) the patina layer is still present on the top of the corrosion products, but it is cracked and has collapsed due to the dissolution of the zinc coating beneath the patina layer. This may lead to a lower intensity of the IR band from the carbonate of $ZnCO_3$ due to increased diffuse scattering of IR light and the presence of cracks. It is also possible that the patina layer is partly transformed into other zinc compounds due to the decrease of pH in the anodic area. An anodic site on the passivated sample showed a similar composition as the other samples (formation of $Zn_5(OH)_8Cl_2 \cdot H_2O$ and $Zn_5(OH)_6(CO_3)$ at the anodic

spot of the sample), which is not shown here.

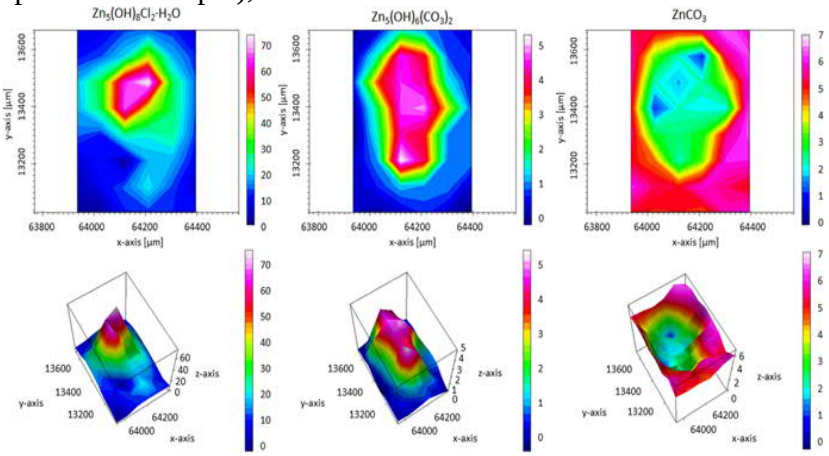


Intensities of IR bands due to $Zn_5(OH)_8Cl_2{\cdot}H_2O$, $Zn_5(OH)_6(CO_3)_2$, and $ZnCO_3$ at a black spot (anodic area) of the patinated sample

# The SEM characterization of black spots/anodic areas

The samples for SEM characterization were taken after 2 days of immersion in the SVET set-up.

## Untreated HDG

OFigure 6 shows SEM images of a black spot that appeared on the reference HDG surface (sample A) after exposure in the SVET set-up for 2 days. The visual appearance of the cavity is consistent with depictions of pitting corrosion in the literature.[6] The cross-section image shows that the zinc layer was locally dissolved all the way to the iron core. It has been reported that the thickness of the metallic zinc layer can decrease significantly on zinc surfaces at anodic areas, whereas there is no decrease in zinc thickness at the cathodic areas (cathodic areas become covered with corrosion products).[15] The cross-section image confirms the corrosion process: at active areas (anodes) on the surface, metal ions are released into solution, producing an ionic current in the solution.[22] At less active areas (cathodes), transportation of electrons from the metal to an acceptor (such as oxygen or hydrogen ions) creates an electronic current in the metal. The presence of $Na^+$ and $Cl^-$ ions assists in transferring ions in the electrolyte solution, which provides the ionic current in the solution that is necessary to sustain the local electrochemical cell.

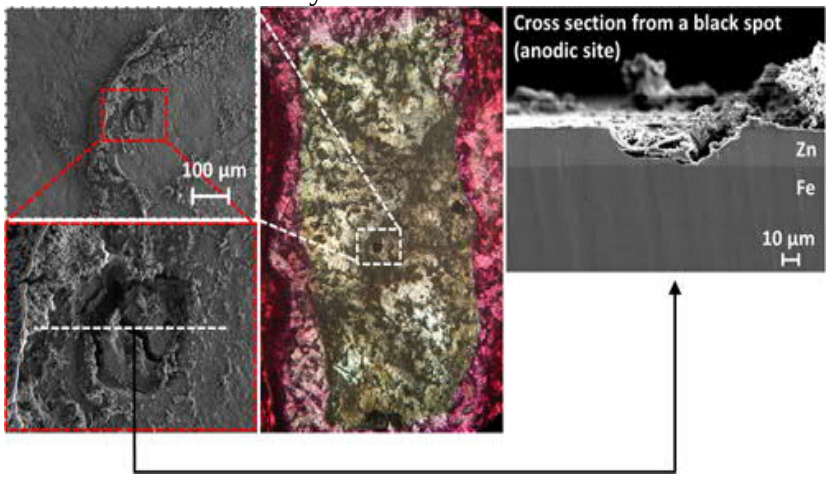

Scanning electron microscopy images of a black spot (anodic site) on the untreated hot-dip galvanized sample (A) after 2 days of immersion in the scanning vibrating electrode technique set-up

## Patinated HDG

SEM images of a black spot on the exposed patina sample (sample B) are shown in OFigure 7. The patina layer was partially collapsed during the exposure at the spot area. The zinc layer was dissolved beneath the patina layer. Element mapping shows that Cl is enriched within the cavity capped by the patina layer (Figure 7). This means that the cavity is populated by secondary corrosion products that contain Cl. The original patina layer is seen as a semi-bright Zn layer covering the secondary corrosion products and the cavity. The bright green area on the left side of the element map overlay corresponds to metallic zinc. In a close-up image (OFigure 8), porous corrosion products can be seen on the top of the steel core. The anodic dissolution process consumed practically the whole zinc layer and stopped at the Al–Fe intermetallic layer between the steel and the original zinc substrate.[8] The underlayer corrosion explains why high current densities were obtained by SVET (Figure 3), but in visual observation, the number of pit initiations on the surface was rather low (Figure 2).

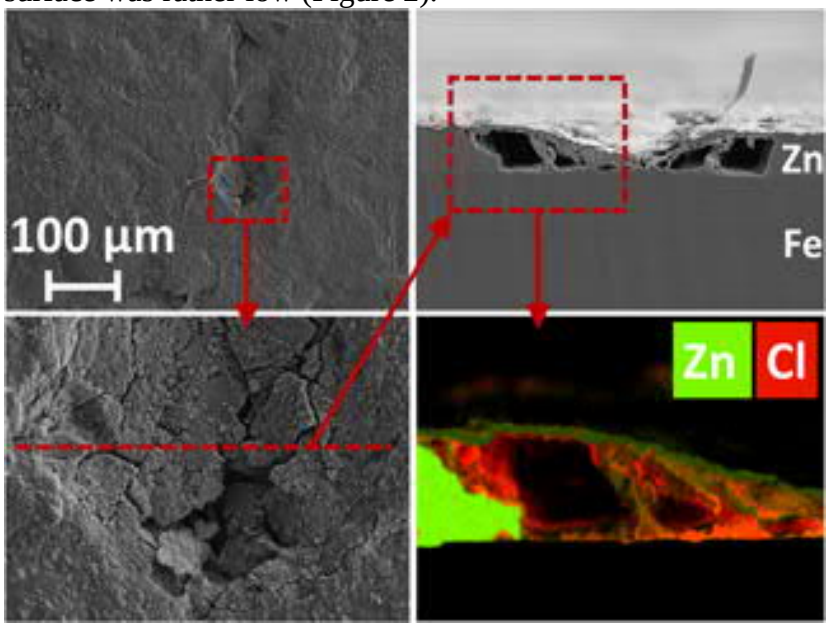


Scanning electron microscopy/energy-dispersive X-ray spectroscopy characterization of a black spot (anodic site) on patinated hot-dip galvanized steel sample after 2 days of immersion in the scanning vibrating electrode technique set-up

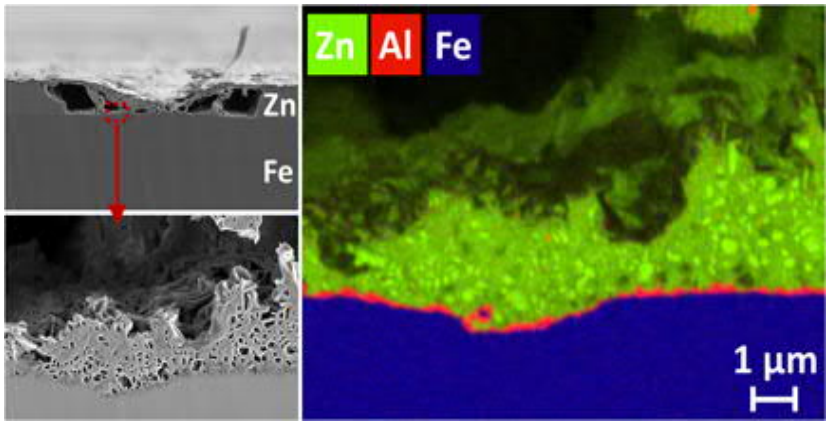


High-resolution element maps of Zn, Al, and Fe on patinated hot-dip galvanized steel sample (B) after 2 days of immersion in the scanning vibrating electrode technique set-up

In the literature, the beneficial role of zinc patina in corrosion inhibition has been attributed to barrier layers containing zinc and carbonate ions.[23] However, the specific roles of zinc corrosion products and the corrosion mechanisms through these barriers are not yet fully understood.[15,17] Zinc patina layers possess high hydrophobicity, which could lead to an efficient barrier against metal corrosion.[20,22] In salt-containing environments, complex zinc corrosion products (not $Zn(OH)_2$ or ZnO), possessing a negatively charged surface, have further been shown to aid in the repulsion of chloride ions[18] and increase the barrier effect against oxygen diffusion.[24] In other studies, this same phenomenon was confirmed by a decrease in oxygen reduction on the surface, measured as a decreased cathodic current, providing clear experimental evidence of the barrier effect.[7,15] Furthermore, there is a great interest in finding sustainable nature-inspired (super)hydrophobic coatings for corrosion barriers of metals.[22,25] However, it is well known that contact between the corrosive solution and the metal/coating interface will corrode the metal surface.[22] The compactness of the patina layer has been shown to correlate with the air permeability and to the corrosion protection better than the thickness of the barrier.[15,26] In addition, an increase in specific surface area, implying pores or cavities in the protective corrosion layer, has been interpreted as a decreased corrosion resistance.[21,27] Thus, the anodic dissolution was probably initiated at a crack or pore in the patina layer. $Cl^-$ ions have been reported to replace $OH^-$ ions in Zn corrosion products via ion exchange reactions.[15,28] However, in this study, the zinc patina layer was anhydrous zinc carbonate, which is less prone to ion exchange and is thus more stable.[23] It is supported by the residual patina layer covering the anodic dissolution site after exposure (Figure 7). It is probable that chloride ions are transported to defects in the patina layer toward the zinc metal layer where corrosion attack is initiated. The cathodic oxygen reduction reaction probably takes place at the zinc surface on defects in the patina layer, such as cracks and pores, as the patina layer itself is a poor cathodic surface. As indicated by the SVET measurements, cathodic areas are present in connection with the anodic spots, on both the untreated HDG and the patina-covered HDG surfaces (Figure 3). The amount of black spots in the immersion experiments (Figure 2) shows that the patinated zinc is less prone to pitting attack, which can be related to a barrier effect of the patina that partly prevents chloride to reach the zinc surface, as well as the effect of the patina to reduce the effective cathodic area. It should be noted that the growth of a substantial amount of chloride-containing corrosion products, $Zn_5(OH)_8Cl_2 \cdot H_2O$, in the pit area, as shown by FTIR imaging and SEM, requires transport of chloride ions through the patina layer to the corrosion front. Hydroxyl ions provided by the cathodic reactions are also transported through the patina layer. A

schematic presentation of these corrosion processes is shown in Figure 9.

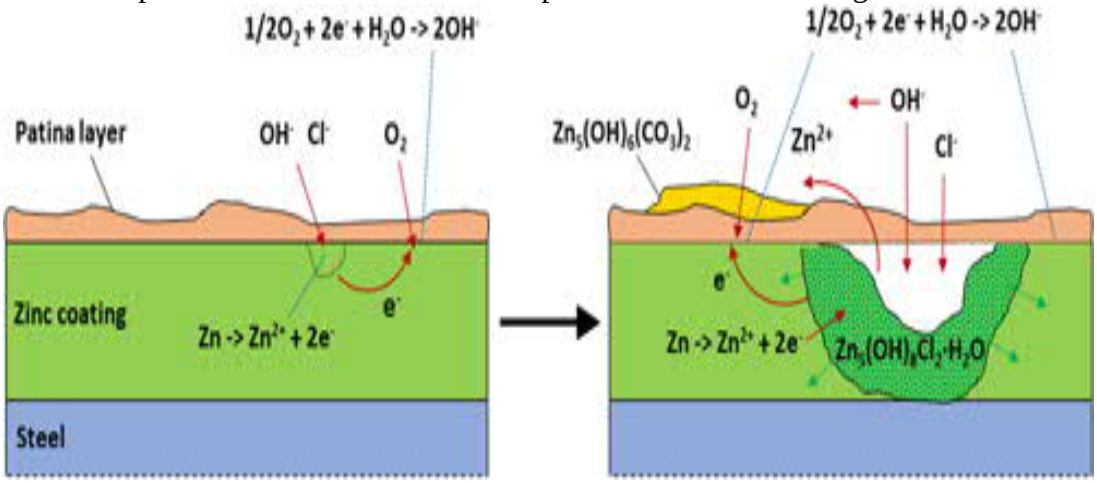


A schematic presentation of the corrosion processes in a patinated hot-dip galvanized sample

## Passivated HDG

The passivated sample exhibited a minor electrochemical activity in an NaCl immersion (Figure 3). A cross-section of the exposed, passivated sample is shown in OFigure 10. The anodic dissolution took place beneath the passivation layer, and Cl was concentrated within the cavity, showing a similar mechanism as the patinated sample. The passivation layer was partly flaking off the zinc surface. The extent of dissolution (visually observed from the thinning of the zinc layer at the anodic spot) was less than that for the patinated sample, showing better barrier properties. In the passivation layer, $Cr^{3+}$ forms $Cr_2O_3$, which functions as a protective barrier on metal.[17] The $Cr^{3+}$-based passivation layer is inherently a barrier lacking the self-healing properties associated with $Cr^{6+}$-based passivations, which means that the long-term corrosion resistance is primarily affected by the sacrificial behavior of Zn and with the corrosion products that passivate the reactive site.[29–31] However, it is clear that the passivation layer constitutes better protection, compared with patina, by reducing the active cathodic area and probably also by the transport of chloride to the reaction front in the zinc layer at the anode.

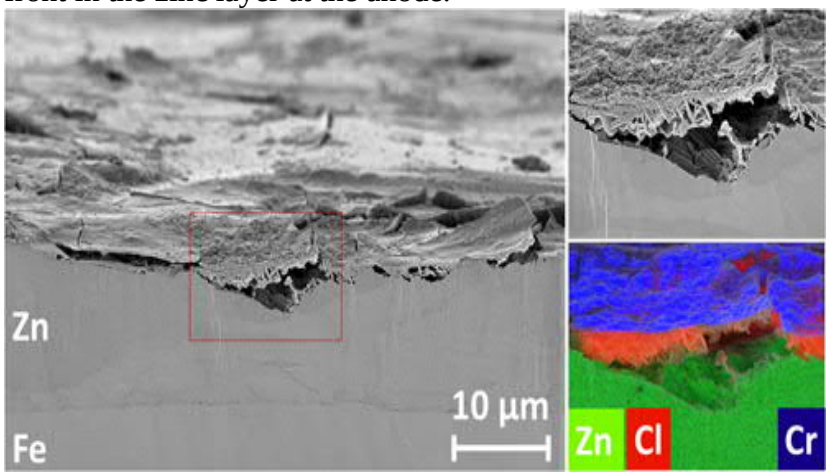


Scanning electron microscopy cross-section images and high-resolution element maps of Zn, Cl, and Cr on a patinated hot-dip galvanized steel sample (C) after 2 days of immersion in the scanning vibrating electrode technique set-up

# SUMMARY AND CONCLUSIONS

Pitting corrosion was induced on untreated, patinated, and passivated HDG by immersing the samples in a 0.1-M NaCl solution. The corrosion currents were monitored by SVET in the electrolyte. The number of black spots (individual pits) was visually calculated from light microscopy images. The untreated HDG sample showed extensive corrosion, seen as a high amount of pits and separation of anodic and cathodic currents over the sample surface. Similarly, the patinated sample showed the formation of anodic spots, but the surface was visually more inert, because the corrosion took place beneath the patina layer. The passivated sample showed the least corrosion. In SEM cross-section images, the anodic spots on untreated HDG showed extensive local zinc dissolution, leaving a cavity in the zinc coating and confirming the pitting corrosion mechanism. The zinc was dissolved all the way to the steel. The dissolution process stopped at the Al–Fe intermetallic layer between the steel core and the original HDG zinc coating, and it continued laterally from the initial pit. In the patinated and passivated samples, the zinc dissolution took place beneath the protective layers. The initial barrier layer could partially collapse (patinated sample) or flake off (passivated sample) due to the extensive dissolution of the substrate. FTIR imaging was performed on samples after exposure, and the distribution of corrosion products was visualized. Cl-containing corrosion products were observed in the anodic areas. FTIR imaging showed the formation of $Zn_5(OH)_8Cl_2{\cdot}H_2O$ and $Zn_5(OH)_6(CO_3)_2$ at the local pits (anodic sites). The localized formation of $Zn_5(OH)_8Cl_2{\cdot}H_2O$ is consistent with the anodic processes, which lead to a local pH decrease that promotes the formation of this phase. The results indicate that the compactness of a layer and the ability to withstand ion exchange and reduce ionic diffusion toward the zinc surface, together with the reduction in the cathodic activity, are important parameters that contribute to the protective properties of surface treatment. A combination of the SVET technique with FTIR imaging provides crucial information on the local corrosion processes and mechanisms of HDG steel samples with different surface treatments. Cross-sections of microscopic pitting corrosion sites that contain porous and abrasion-sensitive corrosion products can be successfully prepared with modern argon ion beam polishing. The latest developments in SEM/EDS technology allow the mapping of nanometer-scale features within these beam-sensitive structures.

# REFERENCES


N. Fuertes, V. Bengtsson, R. Pettersson, M. Rohwerder, Mater. Corros. 2017, 68, 7.

H. Uchida, M. Yamashita, Mater. Sci. Eng., A 2001, 319–321, 496.

R. Akid, D. Roffey, D. Greenfield, D. Guillen, in *Local Probe Techniques for Corrosion Research: European Federation of Corrosion Series* (Eds: R. Oltra, V. Maurice, R. Akid, P. Marcus), Woodhead Publishing, Cambridge, UK 2007, Ch.3.

H. S. Isaacs In: *Electrochemical Society fall meeting*; 1986; pp 2180–2183.

E. Bayet, F. Huet, M. Keddam, K. Ogle, H. Takenouti, Electrochim. Acta 1999, 44, 4117.

X. G. Zhang, Corrosion and Electrochemistry of Zinc, 1st ed., Springer Science+Business Media, LLC, New York, NY 1996.

I. Odnevall, C. Leygraf, in *Atmospheric Corrosion* (Eds: W. Kirk, H. Lawson), ASTM International, West Conshohocken, PA 1995, p.215.

E. McDevitt, Y. Morimoto, M. Meshii, ISIJ Int. 1997, 37, 776.

V. Saarimaa, C. Lange, T. Paunikallio, A. Kaleva, J. P. Nikkanen, E. Levänen, P. Väisänen, A. Markkula, J. Coat. Technol. Res. 2019, 17, 285.

V. Saarimaa, J. Manni, E. Kauppinen, A. Markkula, J. Juhanoja, B.-J. Skrifvars, Surf. Interface Anal. 2014, 46, 620.

V. Saarimaa, A. Kaleva, J. P. Nikkanen, S. Heinonen, E. Levänen, P. Väisänen, A. Markkula, J. Juhanoja, Surf. Coat. Technol. 2017, 331, 137.

G. Angeli, R. Sagl, A. Jarosik, J. Strutzenberger, T. Mörtlbauer, C. Riener, A. Schönauer, Galvatech 2015, 356.

V. Saarimaa, A. Kaleva, J.-P. Nikkanen, S. Heinonen, E. Levänen, P. Väisänen, A. Markkula, J. Juhanoja, Surf. Coat. Technol. 2017, 331, 137.

H. Kaesche, Electrochim. Acta 1964, 9, 338.

J. D. Yoo, K. Ogle, P. Volovitch, Corros. Sci. 2014, 81, 11.

D. Persson, D. Thierry, O. Karsson, Corros. Sci. 2017, 126, 152.

S. Thomas, N. Birbilis, M. S. Venkatraman, I. S. Cole, Corros. Sci. 2013, 69, 11.

T. H. Muster, I. Cole, Corros. Sci. 2004, 46, 2319.

T. Ishikawa, M. Murai, K. Kandori, T. Nakayama, Corros. Sci. 2006, 48, 3172.

V. Saarimaa, A. Kaleva, J.-P. Nikkanen, J. Manni, C. Lange, T. Paunikallio, T. Laihinen, S. Heinonen, E. Levänen, P. Väisänen, A. Markkula, ACS Appl. Mater. Interfaces 2018, 10, 21730.

F. Zhu, D. Persson, C. Thierry, C. Taxen, Corros. Sci. 2000, 56, 1256.

E. Vazirinasab, R. Jafari, G. Momen, Surf. Coat. Technol. 2017, 341, 40.

J. D. Yoo, K. Ogle, P. Volovitch, Corros. Sci. 2014, 83, 32.

I. Suzuki, Corros. Sci. 1985, 25, 1029.

C. Florica, N. Preda, A. Costas, I. Zgura, I. Enculescu, Mater. Lett. 2016, 170, 156.

T. Ishikawa, Corros. Sci. 2007, 49, 2547.

T. Ishikawa, T. Yoshida, K. Kandori, Corros. Sci. 2007, 49, 1468.

H. Tanaka, Y. Takeuchi, T. Ishikawa, T. Nakayama, Corros. Sci. 2011, 53, 2502.

T. Prosek, D. Thierry, Prog. Org. Coat. 2004, 49, 209.

O. D. Lewis, D. Greenfield, R. Akid, R. H. Dahm, G. D. Wilcox, Trans. IMF 2006, 84, 188.

R. Berger, U. Bexell, T. Mikael Grehk, S. E. Hörnström, Surf. Coat. Technol. 2007, 202, 391.

Saarimaa V, Fuertes N, Persson D, et al. Assessment of pitting corrosion in bare and passivated (wet $scCO_2$-induced patination and chemical passivation) hot-dip galvanized steel samples with SVET, FTIR, and SEM (EDS). Materials and Corrosion. 2020;0–0. https://doi.org/10.1002/maco.202011653